Design of Hairpin Winding and Random Winding Stators for High Speed Heavy-Duty Traction Motor

Jianan Jiang[1,2], Tianjie Zou[2], Antonino La Rocca[2], Salvatore La Rocca[2], Chuan Liu[2], Zeyuan Xu[2], Chris Gerada[2], Shaohong Zhu[3], Krzysztof Paciura[3], David Gerada[2]

1: School of Automation, Northwestern Polytechnical University, Xi'an, China

2: *Faculty of Engineering, University of Nottingham,* Nottingham, UK

3: Accelera by Cummins Ltd, Peterborough, UK

***Abstract*—Hairpin winding with rectangularly shaped conductors are gradually replacing random winding wound with stranded wires in electric vehicle (EV) industry. As the new-generation winding technology, hairpin winding features high electromagnetic and thermal performance to meet the step-change requirements on power density and efficiency levels of EV traction motors. To quantitatively analyze the advantages of hairpin winding compared to random winding, in this paper, two interior permanent magnet (IPM) traction motors, with random winding and hairpin winding, respectively, are designed and compared for the same output torque-speed requirement with 350kW peak power, 550Nm peak torque and 15000 rpm peak speed. The overall design process takes into consideration of performance boundaries in multi-physics domain based on global optimization against typical operating points. A detailed comparison of the optimized motors is carried out in terms of geometry dimensions, material usage, power losses, and thermal performance. The comparison results show improvements of 21.6% decrease in overall volume, 17.4% decrease in active mass, 27.1% increase in peak power density and 28.1% increase in continuous current density for the 96-slot IPM design with hairpin winding. Two prototype machines are manufactured, and experimental validation will be conducted in future research work.**

Keywords—traction motor, random winding, hairpin winding, multi-physics optimization, AC losses, power density

I. INTRODUCTION

Environmental concerns and energy crisis prompted the technology advances for development of cost-effective, efficient, and sustainable vehicles. Electrification is becoming irreversible trend within the transportation industry [1]. The remarkable growth of the electric vehicle industry has driven the demand for higher power density (kW/kg or kW/L), higher efficiency, and lower cost ($/kW) traction motors [2-4]. The UK's Advanced Propulsion Centre (APC) has announced the power density targets for electric traction machines in a roadmap developed in 2020. APC aims to reach 8kW/kg in 2025 and 10kW/kg in 2035 [5], which is a step change compared to the presently available motors of 2-5 kW/kg within commercial electric vehicles (EVs) in recent years.

High power density motors are often characterized by high electromagnetic loading and high speed. High performance permanent magnets (PM) together with ferromagnetic materials are generally needed for EV traction motor to feature high magnetic loading. Meanwhile, the increased power losses caused by high current loading pose great challenges to motor's thermal management. When the motor for an EV operates in flux weakening region, the increase in rotation speed leads to additional losses and rotor mechanical stress. Therefore, from the perspective of practical engineering applications, the design and optimization of EV motor becomes inherently a multi-physics task considering electromagnetic performance, thermal and mechanical limitations to ensure the motor's safety and reliability [6-8]. Moreover, as EV motors are typically required to operate in a wide speed range, multiple operating point analyses should be considered in the optimization process.

Due to the contradiction between the two demands of high power density and high efficiency for traction motors, properly selecting and designing the stator windings is crucial as it is the central pivot of energy conversion process, and thus feature highest power loss density in the machine. Among all commonly used winding types, the round random wire-formed winding has the advantages of low cost, and easy production. It has been widely adopted in early-generation EV traction motors such as BWM i3 2016 and Nissan Leaf 2012 [3]. From winding power loss perspective, aalthough the multi-parallel small-sized wire structure eliminates the skin/proximity effects and the corresponding AC loss, the DC loss is still considerable due to the low slot fill factor. In terms of the thermal aspect, the low slot fill factor leads to relatively low equivalent thermal conductivity in stator slots which is not beneficial to heat dissipation. Moreover, the end winding is always formed in a solid part with insulation sleeves covered on the lead wire side making advanced cooling techniques such as oil spray cooling not applicable.

With the increasing requirements on power density level and efficiency, recently many automotive manufacturers have adopted hairpin windings on traction motors. Compared with random windings, hairpin windings have numerous advantages such as higher slot fill factor, lower DC resistance benefit from the compact structure, and better heat dissipation capacity. Moreover, the uniformed end winding structure can be better integrated with advanced cooling methods to have improved thermal performance. In terms of winding losses, on the one hand, high slot fill factor and reasonable transposition contribute to low DC loss and eliminated circulating current loss. On the other hand, the relatively large conductor size leads to prominent skin and proximity loss at high frequency, which reduces the high-speed efficiency of the motor. Existing literature has made a lot of investigation on AC loss calculation and reduction [9-11], and it is of great importance to consider

AC loss optimisation in the design process of motors with hairpin windings.

Although hairpin winding features much better electromagnetic and thermal performance compared to random winding, it is still subject to the disadvantages of less flexible winding configuration and much higher cost. The selection of winding layout requires comprehensive consideration in performance, cost, and manufacturing. Therefore, it is necessary to obtain a comprehensive quantitative comparison between the two types of windings, providing references for practical applications.

In this paper, two high-power (350kW) IPM traction motors with random winding and hairpin winding, respectively, are designed and optimized in multi-physics domain with typical operating points considered. A comparative study of the optimized motors is carried out in terms of geometry dimensions, power losses and thermal performance, to quantitatively analyse the differences between motors using the two types of windings. In Section II, the performance requirements and machine topology are briefly introduced. Parametric models are built in Section III, and a multi-physics optimization process is proposed. The optimized machine performance is highlighted and compared in terms of loss and thermal performance in Section IV.

II. Performance Requirements and Machine Topology

A. Performance requirements

The performance requirements considered in this paper are summarized in TABLE I, which include a base speed of 5000rpm and a max speed of 15000rpm. The continuous and peak torque is required to be 225kW and 350kW, and the DC bus voltage is 720V. The targeted power and torque-speed curve is given in Fig. 1, the constant power speed ratio (CPSR) for continuous operation is 3:1.

TABLE I. Motor Performance Requirement

Requirement	Target
Base speed	5000 rpm
Max speed	15000 rpm
Peak power (30s)	350 kW
Continuous power	225 kW
Peak torque	550Nm
Max continuous/peak current	180 rmsA / 250 rmsA
Peak power density (active parts)	>=7 kW/kg
DC bus voltage	720 V
Outer diameter	< 300mm
Length	< 200mm

B. Machine topology and slot-pole combination

The double-layer IPM topology is selected in this paper. The number of rotor poles is limited by the switching frequency of the inverter. With the consideration that the fundamental frequency of the motor at peak speed <= 1000Hz, the rotor pole number is fixed to be 8.

With pole number fixed in the analyses of this paper, selection of slots per pole per phase (q) for distributed windings becomes a key design element. Generally, higher number of q might be beneficial in terms of reducing torque ripple, core loss and improving heat dissipation capacity. Meanwhile, the number of q is also limited by (or influencing) other factors including motor size, flux leakage and NVH level. Based on the power/torque level of the motors analysed in this paper, the suitable number of q should be 3 or 4 after rapid sizing process, with both power loss behaviour and manufacturability considered. The more commonly adopted option with q=2 has been found not suitable due to excessive rotor loss and winding temperature raising. In this paper, 72 slots (q=3) configuration is selected for random winding motor, while 96 slots (q=4) configuration is selected for hairpin winding motor. The machine geometry is presented in Fig. 2.

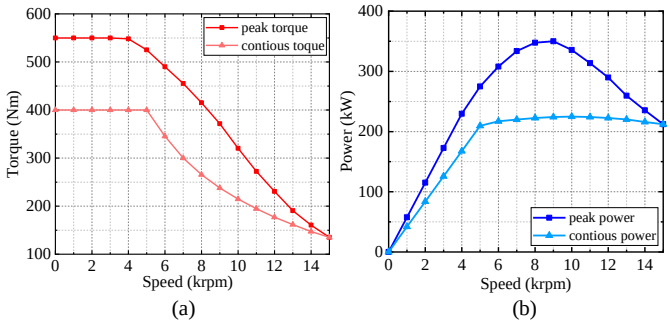

(a) (b)

Fig. 1. Target torque/power vs. speed curve. (a) torque-speed curve; (b) power-speed curve

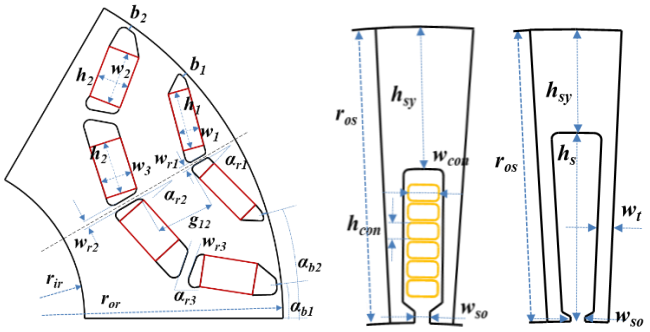

Fig. 2. Parametric rotor and stator modelling with 96-slot (left), 72-slot (right)

C. Parameter setting for fair comparison

To make the comparison more reasonable, some parameters of the motors are discussed as follows.

1)For material selection: High performance electrical steel NO20 and 35HXT780T are adopted on the stator and rotor core respectively ensuring low iron loss and high strength. N42EH has been selected as PM material because of its high energy density and thermal reliability of up to 180°C.

2)For motor geometry: Both motors have the same airgap thickness. The axial length is optimized according to the output torque.

3)For winding manufacturing: The slot fill factor of the random winding motor is set to be 0.38 and that of the hairpin winding motor is 0.64.

4)For cooling technique: Both motors adopt integrated oil cooling (oil spray cooling + water jacket cooling), and the equivalent oil flow rate is 8L/min.

III. MULTI-PHYSICS OPTIMIZATION

As mentioned in Section I, high-power density motors are often characterized by high speed and high electromagnetic loading, which will lead to a sharp increase in various losses, severe heating, and pressure on rotor mechanical strength. In addition, EV traction motors are required to operate in a wide speed range. Therefore, the optimization of such motors is inherently a multi-physics problem covering electromagnetic (EM), thermal and mechanical aspects. Moreover, multiple typical operating points should be covered in the optimization process to obtain the global optimal solution. Three points are chosen for optimization in this paper, which are continuous base speed point(5000rpm, 410Nm), peak power point (8600rpm, 420Nm) and continuous max speed point (15000rpm, 140Nm). The machine optimization process is carried out in ModeFrontier, following the flowchart as shown in Fig. 3.

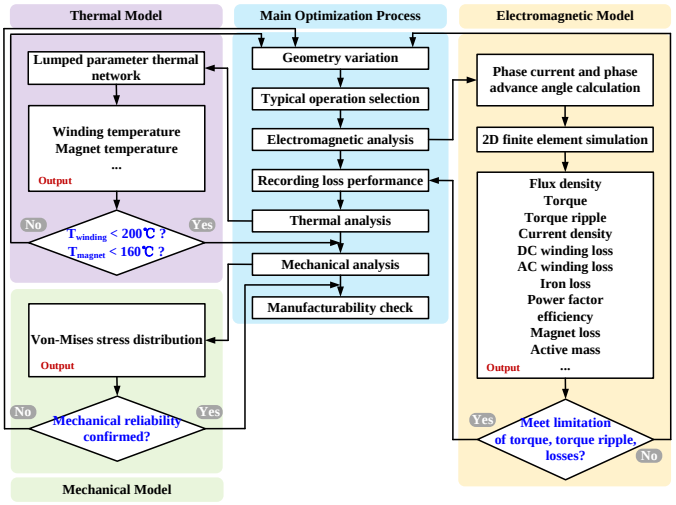

Fig. 3. Multi-physics optimization flowchart

A. Parametric modeling

The electromagnetic performance is calculated in Jmag Designer. Parametric models for the two IPMs are established first for detailed design, as shown in Fig. 2. Six PMs are located into two layers per pole and w_1-w_3, h_1-h_3 denote magnet width and height. Q-axis flux path is determined by the gap g_{12} between two PM layers and the magnet angle α_{r1}, α_{r2}, α_{r3}. The magnetic rib thickness w_{r1}, w_{r2}, w_{r3} affects the d-axis inductance and the strength of the rotor, so they should be designed comprehensively considering the electromagnetic and mechanical performance. The torque ripple is influenced by the magnetic bridge position α_{b1}, α_{b2} which needs to be carefully designed. The number of turns is determined based on the DC voltage constraint. For random winding design, stator tooth width w_t and slot depth h_s determine the slot area and thus the current density. For hairpin winding design, current density is determined by the size of the conductor (w_{con}, h_{con}). All of these parameters are based on reasonable limitations of thermal and mechanical performance.

B. Multi-physic modelling

For different operating points, a preprocessing script is embedded in Jmag Designer to achieve MTPA operation under base speed (5000rpm) for best torque performance and MTPV operation over base speed for lower copper loss. The calculation of AC loss for random winding is a tricky problem because in order to obtain an accurate result, a strand-level FE model should be generated, taking into account the skin and proximity effect and circulating current, which is too time-consuming for the whole optimization process. To balance calculation time and efficiency, a frequency-varying AC loss factor k_{ac} is applied:

$$P_{AC} = k_{ac}(f) * P_{DC} \tag{1}$$

While the AC loss of hairpin winding is estimated by FEM conductor in Jmag Designer ignoring the skin and proximity effect in the end winding.

For thermal calculation, a 3D Lumped Parameter Thermal Network (LPTN) is built in this paper for each motor to quickly obtain the temperature distribution, especially for the stator windings. The connections between each node in LPTN are built basically based on heat conservation equation (2) [12]:

$$q_i + \sum_{j \neq i}^{n} \frac{T_j - T_i}{R_{ij}} = 0 \tag{2}$$

Where R_{ij} is the thermal resistance between node i and node j, and T_i, T_j represent the temperature of adjacent nodes, while q_i is the heat loss generated in node i. According to the arrangement of random winding and hairpin winding within the slot, an equivalent slot thermal conductivity is calculated for random winding based on the proportion of copper, insulation and resin within the slot [13], and the individual thermal resistance of each conductor inside the slot is calculated for hairpin winding motor [12]. To calculate the heat transfer coefficient of water jacket cooling, the following equations are applied [14]:

$$N_u = \frac{(f/8)\times(R_e - 1000)\times P_r}{[1+12.7\times(f/8)^{0.5}\times(P_r^{2/3}-1)]} \tag{3}$$

$$h = \lambda N_u / D_h \tag{4}$$

$$f = (0.79\times\ln(R_e) - 1.64)^{-2} \tag{5}$$

Where λ is the thermal conductor if the coolant, R_e is the Reynolds number, P_r is the coolant Prandtl number, and D_h is the hydraulic diameter which is decided by the cross-section and peripheral length of the cooling channel. For end winding cooling, the heat transfer characteristics are too complicated to estimate, so an estimation approach provided in [12,15] is applied in this paper based on previous experimental work.

The mechanical analysis is carried out in Jmag Designer mainly considering the stress distribution in the rotor under max speed. The thickness of all magnetic bridges and ribs w_{r1}, w_{r2}, w_{r3}, b_1,b_2 has a significant influence on the rotor Von-Mises stress distribution. Hence they should be designed carefully under the mechanical strength limitation.

IV. COMPARISON OF THE OPTIMIZED MOTOR

In this section, the performance of the optimized motors with two winding types is compared in terms of geometry dimensions, flux density, loss characteristics, torque/power

performance, temperature distribution in the slot and Von-Mises stress on the rotor.

Follow the procedure in Section III, the finalized designs of the two motors are summarized in TABLE II. For both motors, appropriate margin has been maintained on output torque & power compared with the requirements in TABLE I. As can be seen from the table, the stator outer diameter of hairpin winding case is 8.3% smaller than that of random winding case, and the stack length is 6.7% smaller. The significant reduction in radial and axial size of the hairpin winding motor is mainly due to its relatively high slot fill factor and electrical loading. Fig. 4 shows the flux density distributions of the two IPMs under the open-circuit condition. The flux leakage is constrained by the saturated magnetic bridge, and the saturation conditions of the two motors are relatively similar and reasonable.

TABLE II. DESIGN SUMMARY OF THE OPTIMIZED MACHINES

Parameters	72-slot	96-slot
Winding topology	Random winding	Hairpin winding
Stator outer diameter, mm	288	264
Rotor outer diameter, mm	190	
Stack length	150	140
Winding configuration	6-phase, 8-turns	6-phase, 6-layer
Continuous power, kW	300	305
Peak power, kW	366	384
Continuous torque, Nm	444	446
Peak Torque, Nm	603	616
Total/DC loss ratio at 15000rpm	1.91	1.43
Active mass. kg	59.6	49.2

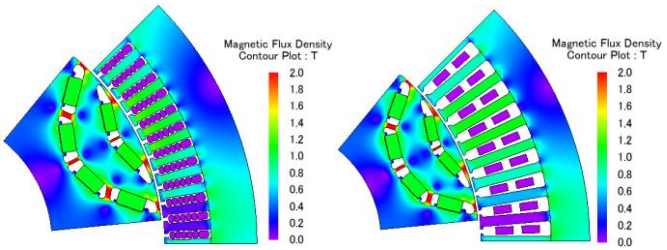

(a) (b)

Fig. 4. No load flux density distribution. (a) 96-slot, hairpin winding; (b) 72-slot, random winding

To achieve a more accurate estimation of random winding AC loss for a fair comparison, a strand-level FE model is built, as shown in Fig. 5 (a). Each bundle is displaced along the tangential direction and the area close to slot opening keeps un-wound to ensure relatively lower AC loss. Fig. 6 shows the current shared by each strand with 1000Hz current input, and it is obvious that the currents in the strands are unevenly distributed and displaced with time.

For random windings, the AC loss caused by the skin/proximity effect is negligible even at 1000Hz due to small sized wires. However, the circulating current loss between strands accounts for a large part of the winding AC losses and increases significantly with frequency because of the great difference in impedance of each strand. Fig. 7 shows each AC loss component at different frequencies for the two winding types, and the input current remains the same (I_{rms}=180A). It should be noted that phase advance has been carefully calculated with DC bus voltage considered. As can be seen, circulating current losses of the 72-slot motor account for 86.9% of the total AC losses at 1000Hz, while the skin/proximity loss accounts for only 13.1%. On the other hand, for hairpin windings, reasonable transposition of the winding eliminates circulating current loss. Meanwhile, due to the large cross-sectional area of the conductors, the skin and proximity effect are the main sources of AC loss.

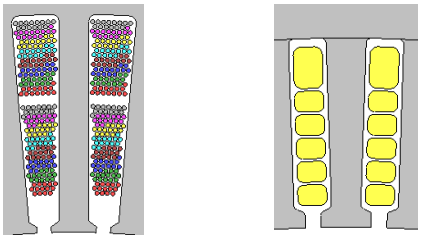

(a) (b)

Fig. 5. FE model of the two motors for AC loss calculation. (a) 72-slot, strand-level FE model; (b) 96-slot, conductor-level FE mode

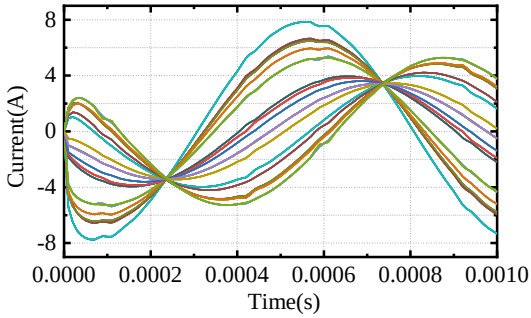

Fig. 6. Current in each strand.

TABLE III. COMPARISON OF AC LOSS AT DIFFERENT FREQUENCIES

Slot-pole	72-8	96-8
Winding topology	Random winding	Hairpin winding
Parallel strands	14	-
Total/DC loss, 0.33kHz	1.10	1.11
Total/DC loss, 600kHz	1.34	1.17
Total/DC loss, 1kHz	1.91	1.43

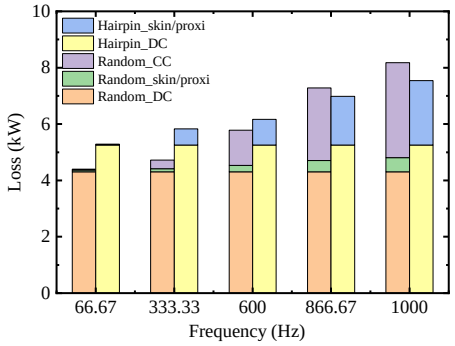

Fig. 7. AC loss components at different frequencies.

Fig. 8 shows the comparison of iron losses in different parts of the two designs at different frequencies. As can be seen from these figures, under the same fundamental frequency, compared to the 72-slot motor, the 96-slot case features higher stator loss density, which is due to the increase in stator slot number leading to an increase in slot flux leakage and slot harmonic. However, The 72-slot design has a higher total stator loss, which is determined by its relatively large stator volume. In terms of the rotor loss, the 96-slot motor features much lower loss as its increased harmonic intensity and the harmonic order of the magnetic field lead to less harmonic flux penetration depth. This can also be noticed in Fig.9, where compared to the 72-slot design, the iron loss of the 96-slot case is more distributed on the outer surface of the rotor.

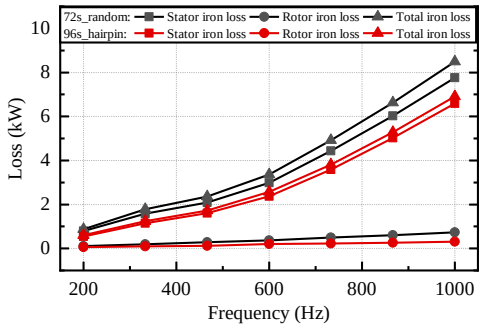

Fig. 8. Iron loss comparison between the two motors.

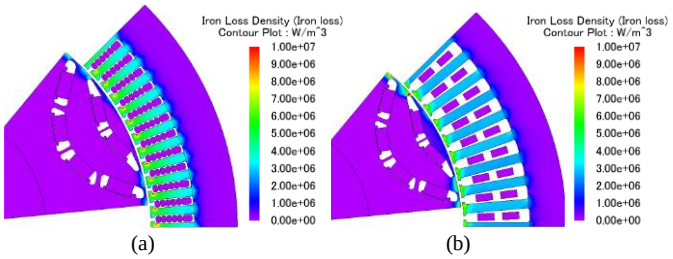

Fig. 9. Iron loss distribution at peak speed operating point (*f*=1000Hz). (a) 96-slot motor; (b) 72-slot motor

Fig. 10 further shows the comparison of efficiency maps based on the 72- and 96-slot designs. For each design, winding loss with ac effect is considered and iron loss with a build factor of 1.5 has been calculated. 720V bus voltage and 250A rms peak phase current have been configured. The peak torque of the 96-slot design is higher than that of the 72-slot case mainly due to its slightly lower d-axis inductance. It can be seen from the figure that the 96-slot motor with hairpin winding has a relatively wider range of high-efficiency area compared to the 72-slot design with random winding due to its lower winding and iron loss. In the low-speed area, DC loss as the dominant loss component of 72-slot case is lower than that of 96-slot case due to its relatively low current density, resulting in higher efficiency.

Fig. 11 shows the temperature distribution of the two motors with integrated oil cooling. Corresponding power losses are obtained based on 5000rpm, 410Nm continuous operation. The current density of the random winding motor and hairpin winding motor is 11.3A/mm2 and 14.5A/mm2, respectively. It can be seen that the hairpin winding features around 10℃ reduced peak temperature in the slot because of its better heat transfer capability even though its current density is higher. Fig. 12 shows the mechanical stress distribution of the optimized rotors at a rotation speed of 16500rpm which is 10% higher than the max speed, and both motors have reasonable margins considering the material yield strength of 840Mpa.

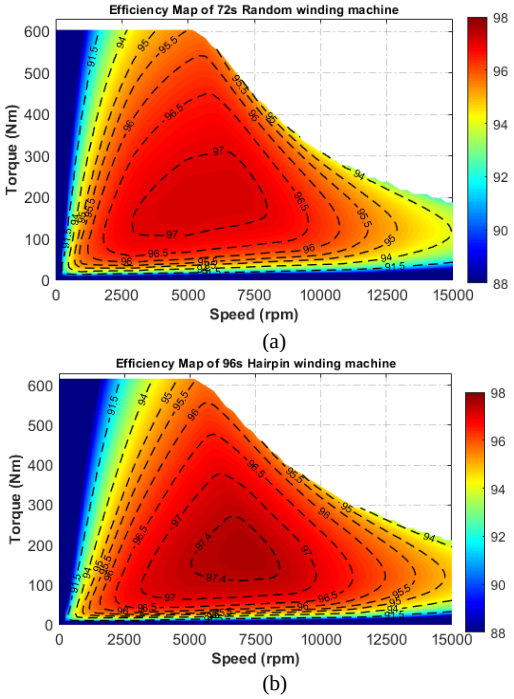

Fig. 10. Comparison of the efficiency maps between the selected (a) 72-slot case with random winding and (b) 96-slot case with hairpin winding.

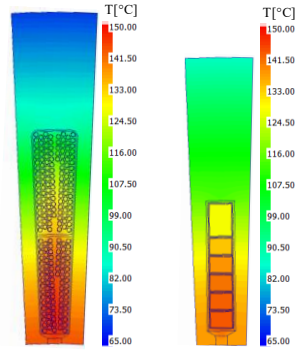

Fig. 11. Temperature distribution in stator slot of IPMs with random winding (left) and hairpin winding (right)

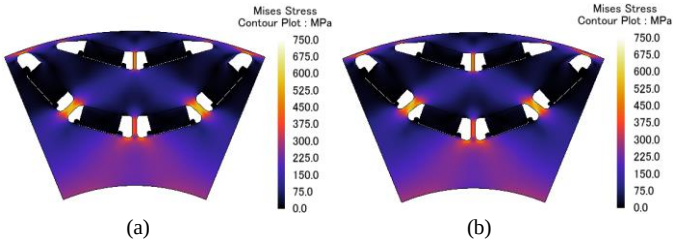

Fig. 12. Von Mises stress of optimized rotors at 16500rpm. (a) 72-slot IPM rotor; (b) 96-slot IPM rotor

The overall comparison between the two motors in terms of geometry dimensions, active mass, slot fill factor, continuous

current density and AC loss ratio is summarized in Table IV. From the table, we can see that compared to the motor with random windings, that with hairpin windings have a 27.1% increase in power density, a 17.4% decrease in active mass and a 68.4% increase in slot fill factor. At the same operating point, the continuous current density increases by 28.1% while the AC loss ratio at max speed decreases by 25.1%. Thus, hairpin winding has shown great advantages in the application of high power heavy-duty traction motors.

TABLE IV. COMPARISON BETWEEN THE TWO MOTORS

Slot-pole	72-8	96-8	Improvement
Winding topology	Random winding	Hairpin winding	
Stator outer diameter, mm	288	264	-8.3%
Stack length, mm	150	140	-6.7%
Motor volume, L	9.8	7.7	-21.6%
Active mass, kg	59.6	49.2	-17.4%
Slot fill factor	0.38	0.64	+68.4%
Continuous current density, A/mm^2	11.3	14.5	+28.1%
Total/DC loss, 1kHz	1.91	1.43	-25.1%
Peak power density, kW/kg	6.1	7.8	+27.1%

V. CONCLUSION

In this paper, two IPM traction motors, with stranded random winding and hairpin winding respectively, are designed and compared for the same output torque-speed requirement with 350kW peak power, 550Nm peak torque and 15000 rpm peak speed, considering performance boundaries in multi-physics domain based on global optimization against typical operating points. A detailed comparison has been made between the two winding topologies in terms of geometry dimensions, loss, electromagnetic, thermal and mechanical performance. The final quantitative results have shown great advantages of hairpin windings in the application of high-power heavy-duty traction motors.

(a) (b)

Fig. 13. Stator windings of prototype machines. (a) 96-slot, hairpin winding; (b) 72-slot, random winding

Two prototype machines with integrated inverter and cooling units have been manufactured following the finalized designs as summarized in Table II, and Fig. 13 shows the two prototyped stator windings. Experimental validation on electromagnetic and thermal performance will be carried out based on further research work.

ACKNOWLEDGEMENT

The authors would like to thank POWERSYS for providing JMAG software as FEA packages for electric machine optimization, and for their support to carry out this research.

The authors would also like to appreciate the support from Cummins Ltd UK in designing and manufacturing the prototype.

This work was supported by the Marie Skłodowska-Curie Actions (MSCA) under the European Union's Horizon 2020 Research and Innovation Staff Exchange (RISE) under Grant 872001.

REFERENCES

[1] J. de Santiago et al., "Electrical Motor Drivelines in Commercial All-Electric Vehicles: A Review," in IEEE Transactions on Vehicular Technology, vol. 61, no. 2, pp. 475-484.

[2] T. Zou et al., "A Comprehensive Design Guideline of Hairpin Windings for High Power Density Electric Vehicle Traction Motors," in IEEE Transactions on Transportation Electrification, vol. 8, no. 3, pp. 3578-3593, Sept. 2022.

[3] I. Husain et al., "Electric Drive Technology Trends, Challenges, and Opportunities for Future Electric Vehicles," in Proceedings of the IEEE, vol. 109, no. 6, pp. 1039-1059, June 2021.

[4] C. Shaw. et al., "Electric vehicles: driving the transition", Fourteenth Report of Session 2017–19, Business, Energy and Industrial Strategy Committee, House of Commons, UK. Oct 2018.

[5] N. Jackson, B. Mecrow, et al., "Electric Machines Roadmap2020", Advanced Propulsion Centre (APC), UK. Feb 2021, Online] Available: https://www.apcuk.co.uk/technology-roadmaps/.

[6] X. Zhu, Z. Xiang, L. Quan, W. Wu and Y. Du, "Multimode Optimization Design Methodology for a Flux-Controllable Stator Permanent Magnet Memory Motor Considering Driving Cycles," in IEEE Transactions on Industrial Electronics, vol. 65, no. 7, pp. 5353-5366, July 2018.

[7] D. Golovanov, L. Papini, D. Gerada, Z. Xu and C. Gerada, "Multidomain Optimization of High-Power-Density PM Electrical Machines for System Architecture Selection," in IEEE Transactions on Industrial Electronics, vol. 65, no. 7, pp. 5302-5312, July 2018.

[8] S. -W. Hwang, J. -Y. Ryu, J. -W. Chin, S. -H. Park, D. -K. Kim and M. -S. Lim, "Coupled Electromagnetic-Thermal Analysis for Predicting Traction Motor Characteristics According to Electric Vehicle Driving Cycle," in IEEE Transactions on Vehicular Technology, vol. 70, no. 5, pp. 4262-4272, May 2021.

[9] X. Ju, Y. Cheng, B. Du, M. Yang, D. Yang and S. Cui, "AC Loss Analysis and Measurement of a Hybrid Transposed Hairpin Winding for EV Traction Machines," in IEEE Transactions on Industrial Electronics, vol. 70, no. 4, pp. 3525-3536.

[10] S. -H. Park, J. -W. Chin, K. -S. Cha, J. -Y. Ryu and M. -S. Lim, "Investigation of AC Copper Loss Considering Effect of Field and Armature Excitation on IPMSM With Hairpin Winding," in IEEE Transactions on Industrial Electronics, vol. 70, no. 12, pp. 12102-12112.

[11] E. Preci et al., "Segmented Hairpin Topology for Reduced Losses at High-Frequency Operations," in IEEE Transactions on Transportation Electrification, vol. 8, no. 1, pp. 688-69.

[12] F. Zhang et al., "A Thermal Modeling Approach and Experimental Validation for an Oil Spray-Cooled Hairpin Winding Machine," in IEEE Transactions on Transportation Electrification, vol. 7, no. 4, pp. 2914-2926, Dec. 2021.

[13] S. Nategh, A. Krings, O. Wallmark, and M. Leksell, "Evaluation of impregnation materials for thermal management of liquid-cooled electric machines," IEEE Transactions on Industrial Electronics, vol. 61, no. 11, pp. 5956-5965, 2014.

[14] V. Gnielinski, "New equations for heat and mass transfer in turbulent pipe and channel flow," Int. Chem. Eng., vol. 16, no. 2, pp. 359–368. 1976.

[15] C. Liu et al., "Estimation of Oil Spray Cooling Heat Transfer Coefficients on Hairpin Windings With Reduced-Parameter Models," in IEEE Transactions on Transportation Electrification, vol. 7, no. 2, pp. 793-803, June 2021.